

Running title: “Transient Turing patterns”.

Transient Turing patterns in a neural field model

A.J. Elvin,* C.R. Laing, and M.G. Roberts

Institute of Information and Mathematical Sciences, Massey University,

Private Bag 102-904, NSMC, Auckland, New Zealand

(Dated: November 5, 2008)

Abstract

We investigate Turing bifurcations in a neural field model with one spatial dimension. For some parameter values the resulting Turing patterns are stable, while for others the patterns appear transiently. We show that this difference is due to the relative position in parameter space of the saddle-node bifurcation of a spatially-periodic pattern, and the Turing bifurcation point. By varying parameters we are able to observe transient patterns whose duration scales in the same way as type-I intermittency. Similar behaviour occurs in two spatial dimensions.

PACS numbers: 87.10.-e, 89.75.Kd

*Author’s current address: Department of Mathematics, The University of Auckland, Private Bag 92019, Auckland, New Zealand

*Email: a.elvin@math.auckland.ac.nz

I. INTRODUCTION

Spatio-temporal pattern formation in regions of the brain has been a topic of great interest for a number of years [1, 2, 4–6, 10, 12, 16, 18, 25, 29]. Because of the relative spatial scales of the patterns of activity and individual neurons, continuum models, in which space is taken as a continuous variable, are often used. The patterns studied include spatially-localised “bumps”, modelling working memory and feature selectivity in the visual cortex [14, 16, 23], travelling waves [12, 24], and spatially-periodic patterns [7, 17, 28].

The formation of periodic patterns in the visual cortex has been proposed as the mechanism behind geometric patterns perceived during hallucinations [3, 10, 11, 26], and a common mechanism for the formation of spatio-temporally periodic patterns is a Turing bifurcation in which a spatially-uniform solution becomes unstable to spatially-periodic perturbations with a range of wavelengths [27]. Such bifurcations in neural field models have been studied by several authors [6, 17, 25, 28, 29].

In this paper we are interested in pattern formation beyond a Turing instability in the model of Laing *et al.* [21]

$$\frac{\partial u(x, t)}{\partial t} = -u(x, t) + \int_{\Omega} w(x - y) f[u(y, t)] dy \quad (1)$$

where

$$w(x) = e^{-b|x|}(b \sin |x| + \cos x) \quad (2)$$

and

$$f(u) = 2H(u - \theta)e^{-r/(u-\theta)^2} \quad (3)$$

where H is the Heaviside function. Here, $u(x, t)$ is the average voltage, or activity level, of a neuronal population at spatial position x and time t . The parameter b governs the rate at which oscillations in the coupling function w decay with distance. The firing rate function f in (3) models neurons firing once threshold is reached and tends to a maximal limit as the stimulus is increased. Parameter θ is the firing threshold and r is the steepness parameter.

The main difference between this model and those previously studied is the form of the coupling function, which is oscillatory rather than of “Mexican-hat” type [4, 10]. This decaying oscillatory form was motivated by labelling studies showing that

spatially approximate periodic stripes are formed by coupled groups of neurons in the prefrontal cortex [15]. Only spatially-localised patterns have previously been studied for this model [19, 21], and the oscillatory nature of the coupling function is likely to lead to novel behaviour [20].

Our goal is to use the analytical stability analysis of Hutt *et al.* [17] to investigate Turing instabilities in (1)–(3). Since the trigonometric functions in w have period 2π we choose a domain $\Omega = [-10\pi, 10\pi]$, with periodic boundary conditions. (The effects of a different domain size are discussed below). In (2) and (3), we have $b, \theta > 0$ and set $r = 0.095$.

The paper proceeds as follows. First, we find spatially-uniform steady states of the model in (1)–(3). We then use linear stability analysis to find regions of parameter space where Turing instabilities can occur. In Section II C numerical simulations of the full model show that spatially-uniform steady states can go unstable to both stable and transient Turing patterns, depending upon parameter values. Through bifurcation analysis of periodic patterns we find that the stability of Turing patterns is due to the position of the saddle-node bifurcation of a spatially-periodic pattern in relation to the parameter value at which the Turing instability occurs. In Section II E we show that the transiency of some solutions is related to type-I intermittency, and in Section II F we extend the analysis to two spatial dimensions. The appendix contains details of the numerical continuation of periodic orbits.

II. ANALYSIS AND RESULTS

A. Spatially-uniform states

We first find spatially-uniform steady states of (1)–(3). Let u^* be the value of u at one of these states. Since $\theta > 0$, one solution is $u^* = 0$. Nontrivial values of u^* satisfy

$$u^* = Wf(u^*)$$

where

$$W \equiv \int_{\Omega} w(x)dx = \frac{4b(1 - e^{-10b\pi})}{b^2 + 1},$$

that is,

$$u^* = \frac{8b(1 - e^{-10b\pi})e^{-r/(u^* - \theta)^2}}{b^2 + 1}. \quad (4)$$

Given b , (4) has one or three solutions, depending upon the value of θ . Fig. 1 shows u^* as a function of θ . With respect to spatially uniform perturbations, the zero and upper steady states are always stable (solid lines) and the middle steady state is unstable (dashed lines). The two nonzero steady states are destroyed in a saddle-node bifurcation as θ increases.

B. Stability

To find a possible Turing bifurcation point we use the linear stability analysis of Hutt et al. [17]. Let u^* to be the upper spatially-uniform steady state found in (4) and let

$$u(x, t) = u^* + \sum_{n=-\infty}^{\infty} u_n \exp(ik_n x + \lambda_n t)$$

where $k_n = 2\pi n/|\Omega| = n/10$. Substituting into (1) and keeping first order terms we obtain

$$\lambda_n = -1 + \gamma W_n$$

where $\gamma \equiv f'(u^*)$ and

$$W_n = \frac{4b(b^2 + 1) [1 - (-1)^n e^{-10b\pi}]}{(b^2 + k_n^2)^2 + 2(b^2 - k_n^2) + 1}.$$

We see that $\lambda_n \in \mathbb{R}$, so no oscillatory bifurcations are expected. Bifurcations do occur when $\lambda_n = 0$, that is, when

$$\gamma = \gamma^* \equiv \frac{1}{W_n} = \frac{(b^2 + k_n^2)^2 + 2(b^2 - k_n^2) + 1}{4b(b^2 + 1) [1 - (-1)^n e^{-10b\pi}]}. \quad (5)$$

Since $W_n > 0$, the uniform steady state loses stability as γ increases through γ^* . Now $d\gamma^*/dk_n > 0$ for $b > 1$, so in this case u^* will go unstable to a perturbation with $k = 0$, i.e. to another spatially-uniform state. When $0 < b < 1$, $\gamma^*(k_n)$ has a minimum at $k_n = \sqrt{1 - b^2}$, and there will be a spatial pattern of wavelength k_m appearing when $\gamma = \gamma^*(k_m)$, where m is the integer for which $\gamma^*(k_m)$ is minimised over all k_n . Fig. 2 shows γ^* as a function of k_n for $b = 0.25, 0.50, 0.75$. For $b = 0.25$, the horizontal line shows $\gamma = \gamma^*$ and indicates the onset of instability. The unstable wavenumber

is $k_n = 1.0$, hence $n = 10$. (Recalling that $k_n = 2\pi n/|\Omega|$, we see that for a different domain size, periodic perturbations with $n \neq 10$ may be the most unstable.) As θ is varied further, γ increases through γ^* and u^* loses stability to a spatial perturbation. For $b = 0.50$, the dominant unstable wavenumber is $k_n = 0.9$, so $n = 9$. For $b = 0.75$, the dominant unstable wavenumber is $k_n = 0.7$, therefore $n = 7$.

In Fig. 3 we show curves corresponding to Turing bifurcations for $n = 8, 9$ and 10 , over a range of b values. The upper fixed point is stable to the left of the leftmost curve. We see that for $0.47 < b < 0.5$, the uniform steady state goes unstable to a pattern with $n = 9$ as θ is increased, whereas for $0.25 < b < 0.3$, a pattern with $n = 10$ appears. Also shown is the curve of saddle-node bifurcations of the upper and middle spatially-uniform fixed points. To the right of this, these states do not exist.

C. Simulations

We now show the results of simulations of (1)–(3) to confirm the above analysis. We discretise Ω into a uniform grid of 501 points, and the convolution term is approximated by a Riemann sum. We set b and, using (5), choose θ such that the upper nonzero spatially-uniform steady state given by (4) will be unstable to a spatially-periodic pattern through a Turing instability. As an initial condition we use the steady state plus a small random spatial perturbation. A typical Turing pattern that appears is shown in the top panel of Fig. 4. This pattern has $n = 10$, as expected. However, if we choose another set of parameter values, such as $b = 0.5, \theta = 1.94$, we see the behaviour in the bottom panel of Fig. 4. Here a pattern with $n = 9$ emerges, as expected, but it is transient and the system moves eventually to the spatially-uniform zero steady state. This behaviour was unexpected, as (to our knowledge) transient Turing patterns have only been observed in chemical systems [9, 22], and there, the transiency is due to chemical species in a closed system eventually being consumed.

It seems that for b small, there does exist a stable periodic pattern to which the system is attracted once the Turing bifurcation occurs, whereas for larger b , such a stable pattern does not exist. We now investigate this by finding spatially-periodic patterns and following them as parameters are varied.

D. The role of periodic orbits

The computational details of following periodic orbits are given in the appendix. First, we consider $b = 0.25$. The top panel of Fig. 5 shows the solution curves of 8-, 9- and 10-bump periodic solutions. Stable solutions are indicated by solid lines and unstable solutions by dashed lines. As θ is increased, 10-bump solutions are the last to be destroyed in a saddle-node bifurcation. Vertical lines indicate the value of θ for which a Turing instability occurs. The smallest value of θ for which a Turing instability can occur is for instabilities with the wavenumber $k_n = 1.0$, that is, $n = 10$. Thus a 10-bump periodic solution will always arise in a Turing instability for these parameter values. The saddle-node bifurcation of the upper and middle fixed points is given by the circles joined by solid lines. A non-trivial spatially uniform steady state cannot exist to the right of this line. To the left of the solid vertical line, a stable uniform steady state will be unaffected by a spatial perturbation. For θ between the solid vertical line and the saddle-node bifurcation vertical line, a Turing instability can occur and a stable 10-bump solution forms.

Now consider $b = 0.5$. The bottom panel of Fig. 5 shows the solution curves for 8-, 9- and 10-bump periodic solutions. As θ is increased, the saddle-node bifurcation for 10-bump solutions occurs first, then for 8-bump solutions, and finally, for 9-bump solutions. For this larger value of b , stable periodic patterns do not exist where a Turing instability can arise. The dominant unstable wavenumber is $k_n = 0.9$. Thus a Turing instability will give rise to a 9-bump periodic pattern for the range of θ between the vertical lines for the $n = 9$ Turing instability and the saddle-node bifurcation of the two nonzero fixed points. The 9-bump periodic pattern will only be seen transiently as the system moves to the spatially-uniform zero steady state. This provides an explanation for the behaviour seen in Fig. 4. For low values of b , stable periodic patterns exist for the parameter values at which the spatially-uniform state becomes unstable, and it is to those patterns that the system moves. For higher values of b , stable periodic patterns do not exist for values of θ at which the Turing bifurcation occurs; they have been destroyed in saddle-node bifurcations. Thus an approximately periodic pattern arises from the Turing instability, but the system must move to a stable state which is not spatially-periodic, in this case the spatially-uniform state

$u = 0$.

The different types of behaviour are explained by Fig. 6, where we plot saddle-node bifurcations of spatially-periodic patterns, and Turing instabilities, in the (θ, b) plane. There is a value of b , \bar{b} say, at which the first Turing instability ($n = 9$) occurs at the same value of θ at which the 9-bump periodic solution is destroyed in a saddle-node bifurcation. We see that $\bar{b} \approx 0.4828$. Thus for $b > \bar{b}$ only transient patterns appear, while for $b < \bar{b}$ the patterns created in the Turing bifurcation can be stable and hence permanent, or both permanent patterns and unstable (transient) patterns can appear, depending upon the value of θ .

E. Scaling

The transient behaviour described above is caused by the system passing close to a region of phase space in which (for nearby parameter values) there was a corresponding stable periodic pattern. The effect of such a “ghost” is well-known in relation to type-I intermittency [13] and has been described in chemical systems [9]. It can be shown that for fixed b , the length of time spent in the vicinity of the previously stable structure (in this case, a periodic pattern) scales as $(\theta - \theta^*)^{-1/2}$, where the periodic pattern is destroyed in a saddle-node bifurcation as θ increases through θ^* .

The easiest place to observe this scaling is for b slightly less than \bar{b} , since we can then make $\theta - \theta^*$ arbitrarily small, and have the spatially-uniform state unstable to spatially-periodic perturbations. We set $b = 0.4825$, vary θ near θ^* and measure T , the length of time for which a transient 9-bump structure is present. In Fig. 7 we show $\ln(T)$ versus $\ln(\theta - \theta^*)$, together with the least-squares fit straight line through the data points. The straight line has slope of -0.50071 , in excellent agreement with the predicted value of $-1/2$ for this type of intermittency. These results show that by tuning parameters of the system, arbitrarily long transients can be produced.

F. Two spatial dimensions

We can extend the analysis to two spatial dimensions but over an infinite domain. The correction term for the finite domain is expected to have a small effect. The

equation for the onset of instability in two dimensions can be obtained from (5) by removing the correction term for the finite domain of $(-1)^n e^{-10b\pi}$ in the denominator and replacing the 1D wavenumber with the norm of the 2D wavenumber.

Turing patterns with some spatial structure are observed in numerical simulations (not shown). We see similar behaviour to the one-dimensional model in that the Turing patterns appear to be stable for small b and transient for large b .

III. CONCLUSION

We have studied pattern formation arising out of Turing bifurcations in a recently-proposed neural field model. In contrast with the results of others [6, 17, 25, 28, 29], transient Turing patterns were observed in some regions of parameter space while stable patterns were found elsewhere. We provided an explanation for this by showing that transient Turing patterns occur in regions of parameter space where no stable periodic patterns exist. By varying parameters we were able to control the amount of time for which a transient structure appeared, and this relationship was quantified using the analysis of Type-I intermittency [13]. Simulations in two spatial dimensions showed the same qualitative behaviour.

Macroscopic models such as the one studied here have had a major impact on the understanding of the possible dynamics of brain regions [4]. Our main result is the observation and analysis of transient Turing patterns. These results suggest that transient patterns perceived during hallucinations may not be the result of homeostatic processes “quenching” activity, but rather a result of the intrinsic dynamics of the system itself.

APPENDIX A: FOLLOWING PERIODIC PATTERNS

Here we show how to follow spatially-periodic patterns in parameter space to determine regions in which they exist and are stable. We represent these periodic patterns using Fourier series:

$$u(x) = \frac{a_0}{2} + \sum_{m=1}^{\infty} [a_m \cos(mk_n x) + b_m \sin(mk_n x)]. \quad (\text{A1})$$

Since the domain is of size 20π we take $w(x)$ to be periodic with period 20π , writing

$$w(x) = \frac{\alpha_0}{2} + \sum_{p=1}^{\infty} \alpha_p \cos(px/10) \quad (\text{A2})$$

where

$$\alpha_0 = \frac{2}{20\pi} \int_{\Omega} w(x) dx = \frac{W}{10\pi}$$

and

$$\begin{aligned} \alpha_p &= \frac{2}{20\pi} \int_{\Omega} \cos(px/10) w(x) dx \\ &= \frac{2b(b^2 + 1)(1 - e^{-10b\pi})}{5\pi\{[b^2 + (p/10)^2]^2 + 2[b^2 - (p/10)^2] + 1\}}. \end{aligned}$$

Substituting (A1) and (A2) into (1) we have

$$\begin{aligned} &\frac{a_0}{2} + \sum_{m=1}^{\infty} [a_m \cos(mnx/10) + b_m \sin(mnx/10)] = \\ &\frac{\alpha_0}{2} \int_{\Omega} f[u(y)] dy + \\ &\sum_{p=1}^{\infty} \alpha_p \cos(px/10) \int_{\Omega} \cos(py/10) f[u(y)] dy + \\ &\sum_{p=1}^{\infty} \alpha_p \sin(px/10) \int_{\Omega} \sin(py/10) f[u(y)] dy. \end{aligned}$$

So for $p = mn$ we have

$$a_0 = \alpha_0 \int_{\Omega} f[u(x)] dx$$

$$a_m = \alpha_{mn} \int_{\Omega} \cos(mnx/10) f[u(x)] dx$$

and

$$b_m = \alpha_{mn} \int_{\Omega} \sin(mnx/10) f[u(x)] dx.$$

Note that since $u(x)$ is periodic with period $20\pi/n$ we have

$$a_0 = n\alpha_0 \int_0^{20\pi/n} f[u(x)] dx \quad (\text{A3})$$

$$a_m = n\alpha_{mn} \int_0^{20\pi/n} \cos(mnx/10) f[u(x)] dx \quad (\text{A4})$$

and

$$b_m = n\alpha_{mn} \int_0^{20\pi/n} \sin(mnx/10) f[u(x)] dx. \quad (\text{A5})$$

Equations (A3)–(A5) form a set of nonlinear coupled equations. These equations do not uniquely specify the solution, since any spatial translation of $u(x)$ is also a solution. We thus pick one from this infinite family by imposing that $a_1 = 0$. We set b and θ , choose n , and find an initial n -bump pattern that is a solution of (1) by solving (A3)–(A5). We use the pseudoarclength continuation method [8] to find solutions as parameter values are varied. Following these patterns as θ is increased, we find that they are destroyed in saddle-node bifurcations, as shown in Fig. 5.

-
- [1] S. Amari, *Biol. Cybern.* **27**, 77 (1977)
 - [2] P. C. Bressloff, N. W. Bressloff and J. D. Cowan. *Neural Comput.* **12** 2473-2511 (2000).
 - [3] P. C. Bressloff, J. D. Cowan, M. Golubitsky, P. J. Thomas and M. Wiener. *Neural Comput.* **14**, 473-491 (2002)
 - [4] S. Coombes, *Biol. Cybern.* **93**, 91 (2005)
 - [5] S. Coombes and M. R. Owen, *Phys. Rev. Lett.* **94**, 148102 (2005)
 - [6] S. Coombes, N. A. Venkov, L. Shiau, I. Bojak, D. T. J. Liley, and C. R. Laing, *Phys. Rev. E* **76**, 051901 (2007)
 - [7] R. Curtu and G. B. Ermentrout, *SIAM J. App. Dyn. Sys.* **3**, 191 (2004)
 - [8] E. J. Doedel, R. C. Paffenroth, A. R. Champneys, T. F. Fairgrieve, Y. A. Kuznetsov, B. E. Oldeman, B. Sandstede and X. Wang, *AUTO 2000: Continuation and bifurcation software for ordinary differential equations (with HomCont)*, Technical Report, Caltech (2001)
 - [9] I. R. Epstein and J. A. Pojman, *An introduction to nonlinear chemical dynamics* (Oxford University Press, 1998)
 - [10] G. B. Ermentrout, *Rep. Prog. Phys.* **61**, 353 (1998)
 - [11] G. B. Ermentrout and J. D. Cowan. *Biol Cybernet* **34** 137-150, (1979).
 - [12] D. Golomb and G.B. Ermentrout. *Phys. Rev. Lett.* **86**, 4179-4182 (2001).
 - [13] J. Guckenheimer and P. Holmes, *Nonlinear oscillations, dynamical systems, and bifurcations of vector fields* (Springer-Verlag New York, Inc., 1983)
 - [14] Y. Guo and C. C. Chow, *SIAM J. App. Dyn. Sys.* **4**, 217 (2005)
 - [15] B. S. Gutkin, G. B. Ermentrout, and J. O’Sullivan, *Neurocomputing* **32–33**, 391 (2000)

- [16] D. Hansel and H. Sompolinsky. Modeling Feature Selectivity in Local Cortical Circuits. In *Methods in Neuronal Modeling: From Synapse to Networks*. Koch C and Segev I, Eds, (MIT Press, Cambridge, MA, 1998), (1998).
- [17] A. Hutt, M. Bestehorn, and T. Wennekers, *Network: Comp. Neur. Sys.* **14**, 351 (2003)
- [18] K. Kang, M. Shelley and H. Sompolinsky. *Proceedings of the National Academy of Sciences USA*, **100**, 2848-2853. (2003)
- [19] C. R. Laing and W. C. Troy, *PDE methods for nonlocal models. SIAM J. Appl. Dyn. Syst.* **2**, pp. 487-516 (2003).
- [20] C. R. Laing and W. C. Troy, Two-bump solutions of Amari-type models of neuronal pattern formation. *Physica D.* **178**, 190-218 (2003).
- [21] C. R. Laing, W. C. Troy, B. Gutkin, and G. B. Ermentrout, *SIAM J. App. Math.* **63**, 62 (2002)
- [22] I. Lengyel, S. Kadar and I. R. Epstein, *Science*, **259**, pp. 493 - 495, 1993.
- [23] M. R. Owen, C. R. Laing, and S. Coombes, *New J. Phys.* **9** (2007)
- [24] K. A. Richardson, S. J. Schiff and B. J. Gluckman. *Physical Review Letters*, **94**, 028103, (2005)
- [25] M. L. Steyn-Ross, D. A. Steyn-Ross, M. T. Wilson, and J. W. Sleight, *Phys. Rev. E* **76**, 011916 (2007)
- [26] P. Tass. *Journal of Biological Physics* **21**, 177-210 (1995).
- [27] A. M. Turing, *Phil. Trans. R. Soc. London Series B* **237**, 37 (1952)
- [28] N. A. Venkov, S. Coombes, and P. C. Matthews, *Phys. D* **232**, 1 (2007)
- [29] J. Wyller, P. Blomquist, and G. T. Einevoll, *Phys. D* **225**, 75 (2007)

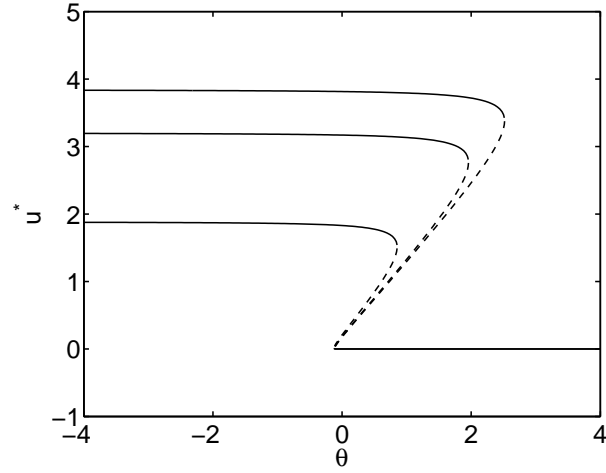


FIG. 1: Spatially-uniform steady states, u^* , of (1)–(3) as a function of θ , as given by (4). The curves from bottom to top are for $b = 0.25, 0.50, 0.75$ respectively.

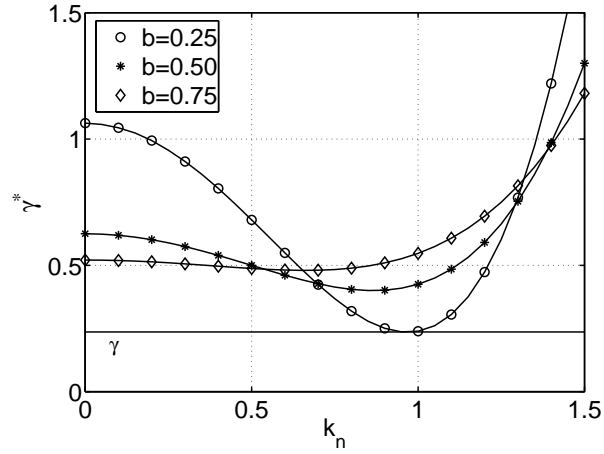


FIG. 2: γ^* as a function of k_n for $b = 0.25, 0.50, 0.75$. The wavenumbers $k_n = n/10$ are indicated by circles, asterisks and diamonds for $b = 0.25, 0.50, 0.75$, respectively. For $b = 0.25$, the horizontal line of γ indicates the onset of instability and a dominant unstable wavenumber of $k_n = 1.0$.

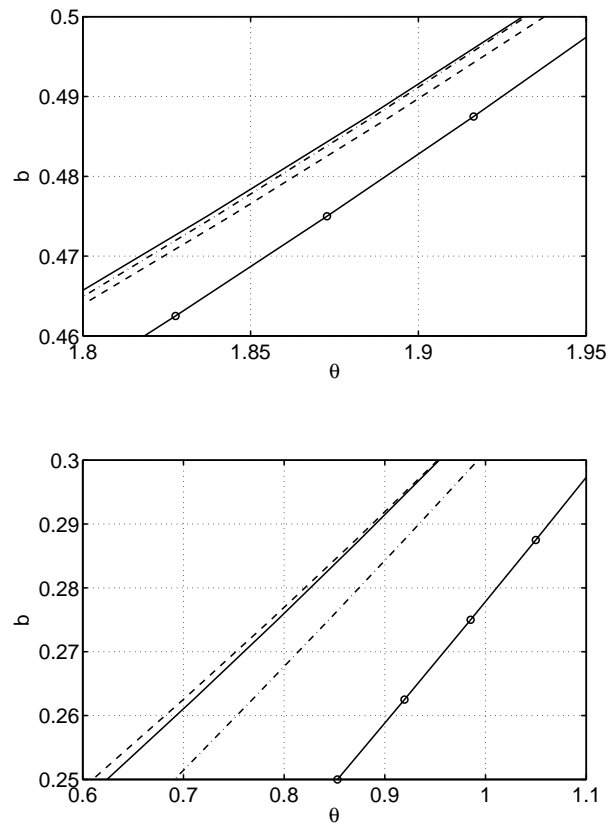


FIG. 3: Curves of Turing instabilities for $n = 8, 9, 10$ (dashed-dot, solid and dashed, respectively). Also shown is the curve of saddle-node bifurcations of the upper and middle fixed points (circles joined by solid line).

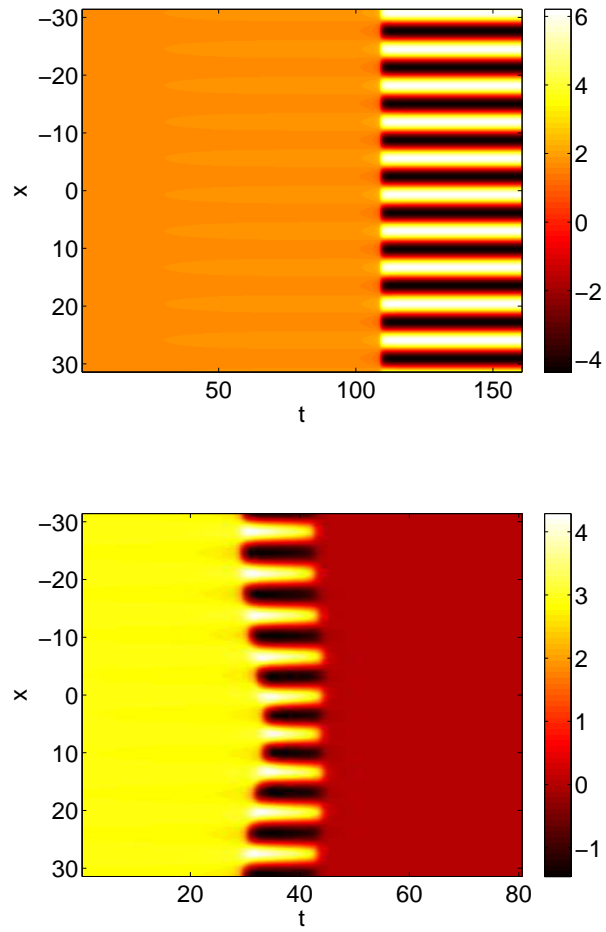


FIG. 4: (Color online) Top: A stable Turing pattern for $b = 0.25, \theta = 0.63$. Bottom: A transient Turing pattern for $b = 0.5, \theta = 1.94$. Time is plotted horizontally and space vertically. The color indicates the value of u (scale on right).

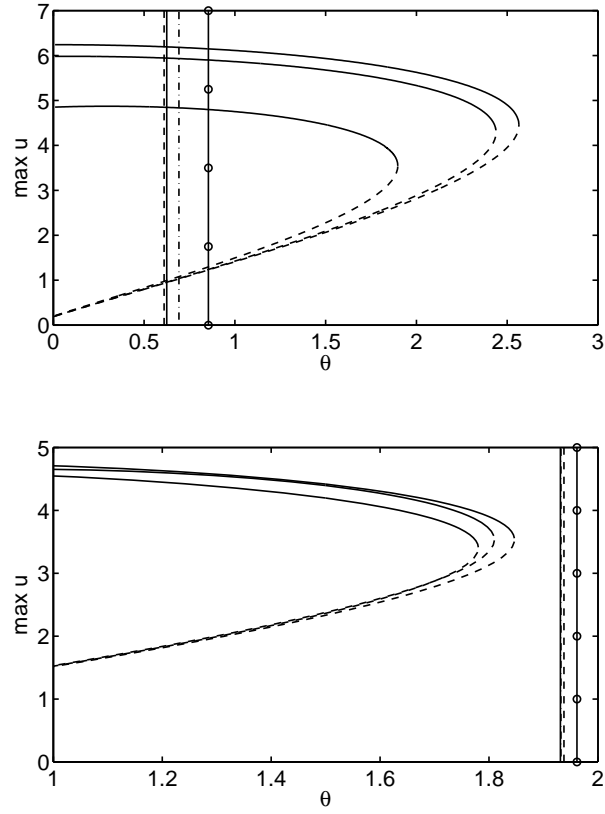


FIG. 5: Top: Solution curves for n -bump periodic patterns for $b = 0.25$ ($n = 10, 9, 8$ from right to left). Solid line for stable solution and dashed line for unstable solution. The vertical lines give the Turing instability for $n = 10, 9, 8$ (dashed, solid, dashed-dot, respectively). Also shown is the curve of saddle-node bifurcations of the upper and middle fixed points (circles joined by solid line). Bottom: Solution curves for n -bump periodic patterns for $b = 0.50$ ($n = 9, 8, 10$ from right to left).

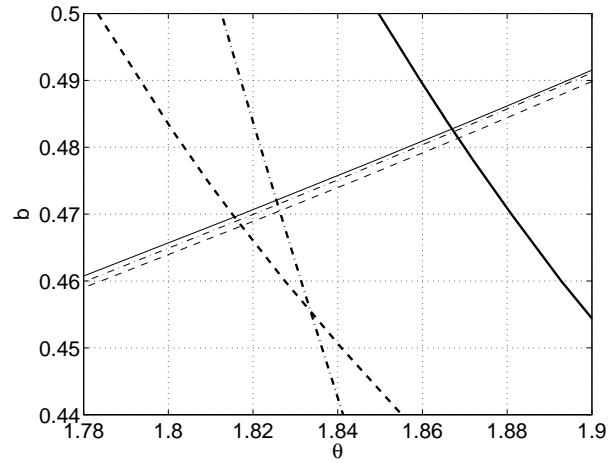


FIG. 6: Curves of saddle-node bifurcations of n -bump periodic patterns (bold lines) and curves of Turing instabilities for $n = 8, 9, 10$ (dashed-dot, solid and dashed, respectively).

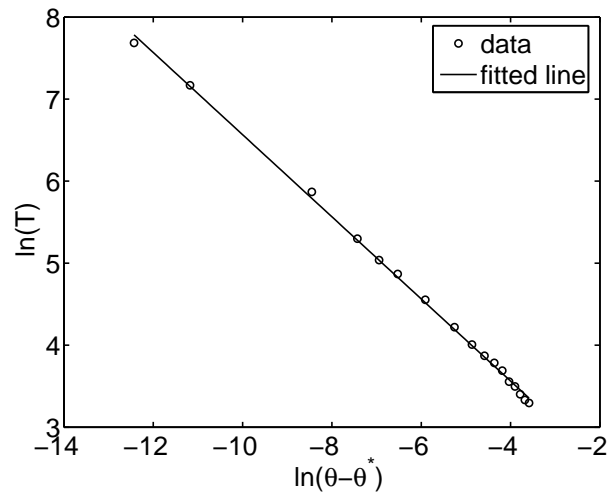


FIG. 7: Plot of $\ln(T)$ as a function of $\ln(\theta - \theta^*)$ where T is the length of time a transient 9-bump structure is present for $b = 0.4825$ and θ . The saddle-node bifurcation of 9-bump periodic patterns occurs at θ^* . The fitted line has a slope of -0.50071 .